Characterization of Uptake of the New PET Imaging Compound ^{18}F-Fluorobenzyl Triphenyl Phosphonium in Dog Myocardium

Igal Madar[1], Hayden T. Ravert[1], Yong Du[1], John Hilton[1], Lana Volokh[1], Robert F. Dannals[1], James J. Frost[1], and Joshua M. Hare[2,3]

[1]Department of Radiology, The Johns Hopkins University School of Medicine, Baltimore, Maryland; [2]Department of Medicine, The Johns Hopkins University School of Medicine, Baltimore, Maryland; and [3]Institute for Cell Engineering, The Johns Hopkins University School of Medicine, Baltimore, Maryland

^{18}F-Labeled *p*-fluorobenzyl triphenyl phosphonium cation (^{18}F-FBnTP) is a member of a new class of positron-emitting lipophilic cations that may act as myocardial perfusion PET tracers. Here, we characterize the ^{18}F-FBnTP uptake and retention kinetics, in vitro and in vivo, as well as the myocardial and whole-body biodistribution in healthy dogs, using PET. **Methods:** Time-dependent accumulation and retention of ^{18}F-FBnTP in myocytes in vitro was studied. Seven anesthetized, mongrel dogs underwent dynamic PET scans of the heart after intravenous administration of 126−240 MBq ^{18}F-FBnTP. In 4 of the 7 dogs, at the completion of a 60-min dynamic scan, whole-body scans (4 bed positions, 5-min emission and 3-min transmission per bed) were acquired. Arterial blood samples were collected at 0, 5, 10, 20, 30, and 60 min after administration, plasma activity was counted, and high-performance liquid chromatographic analyses for metabolites were performed. The extent of defluorination was assessed by measuring ^{18}F-FBnTP bone uptake in mice, compared with ^{18}F-fluoride. **Results:** The metabolite fraction comprised <5% of total activity in blood at 5 min and gradually increased to 25% at 30 min after injection. In vivo, ^{18}F-FBnTP myocardial concentration reached a plateau level within a few minutes, which was retained throughout the scanning time. In contrast, activity in the blood pool and lungs cleared rapidly (half-life = 19.5 ± 4.4 and 30.7 ± 11.6 s, respectively). Liver uptake did not exceed the activity measured in the myocardium. At 60 min, the uptake ratios of left ventricular wall to blood, lung, and liver (mean of 7 dogs) were 16.6, 12.2, and 1.2, respectively. Summation of activity from 5 to 15 min and from 30 to 60 min after injection produced high-quality cardiac images of similar contrast. Circumferential sampling and a polar plot revealed a uniform distribution, near unitary value, throughout the entire myocardium. The mean coefficient of variance, on 30- to 60-min images along the septum-to-anterior wall and the apex-to-base axes was 7.58% ± 1.04% and 6.11% ± 0.89% (mean ± SD; *n* = 7), respectively, and on 5- to 15-min images was 7.25% ± 1.43% and 6.12% ± 1.88%, respectively. ^{18}F-FBnTP whole-body distribution was highly organ specific with the kidney cortex being the major target organ, followed by the heart and the liver. **Conclusion:** ^{18}F-FBnTP is a promising new radionuclide for cardiac imaging using PET with rapid kinetics, uniform myocardial distribution, and favorable organ biodistribution.

Key Words: ^{18}F-FBnTP; heart; PET; imaging

J Nucl Med 2006; 47:1359–1366

Despite recent advances in therapeutic and diagnostic approaches, coronary artery disease (CAD) remains a major health problem worldwide. Nuclear medicine technologies play a key role in the diagnosis and treatment plan design for CAD (*1*). Currently, the SPECT radionuclide ^{201}Tl and the technetium complexes ^{99m}Tc-sestamibi and ^{99m}Tc-tetrofosmin are the mainstay of myocardial perfusion imaging (MPI) tests. However, the absence, at the present time, of a standardized method in the clinic for correction of photon attenuation and the suboptimal spread of technetium tracers in organs adjacent to the heart may result in artifacts interfering with detection of flow abnormalities when using SPECT (*2*). Photon attenuation could prevent an accurate quantitation of tracer uptake, which may be essential for detection of CAD in the absence of regional flow heterogeneity, in cases such as "balanced ischemia" (*3,4*).

PET affords a means of imaging with better temporal and spatial resolution than SPECT and a standardized method for attenuation correction, allowing quantitation of coronary blood flow in absolute terms. Despite the unique advantages of PET and the rapid proliferation of scanners, the use of cardiac PET studies in the clinic is limited. ^{13}N-ammonia and ^{82}Rb are excellent perfusion tracers (*5–7*). However, the need of an on-site cyclotron for ^{13}N-ammonia production and the high cost of a ^{82}Rb generator hinder the more frequent use of PET in clinical MPI studies. Previously, we examined the imaging characteristics of the phosphonium analog ^{11}C-methyltriphenyl phosphonium (^{11}C-TPMP) in dogs using dynamic PET (*8*). ^{11}C-TPMP demonstrated features essential for successful cardiovascular imaging, including rapid clearance from the blood pool, fast accumulation and prolonged

Received Feb. 8, 2006; revision accepted Apr. 26, 2006.
For correspondence or reprints contact: Igal Madar, PhD, JHOC 4230, 601 North Caroline St., Baltimore, MD 21287.
E-mail: imadar@jhmi.edu

retention in the myocardium, and very low lung activity. However, the short physical half-life of ^{11}C renders ^{11}C-TPMP impractical for routine clinical MPI studies. A perfusion PET tracer labeled with ^{18}F may address some of the limitations indicated.

Recently, a series of analogs of TPMP labeled with ^{18}F was developed. (*9*). So far, the radioligand ^{18}F-fluorobenzyl triphenyl phosphonium (^{18}F-FBnTP) demonstrated the most promising characteristics as an imaging tracer. In this study, we characterized ^{18}F-FBnTP metabolic stability, the uptake kinetics in isolated myocytes and in dog myocardium, as well as the myocardial and whole-body distribution in dogs, using PET.

MATERIALS AND METHODS

Preparation of ^{18}F-FBnTP

^{18}F-FBnTP was prepared as described (*9*). Briefly, ^{18}F-fluoride and *p*-trimethylammoniumbenzaldehyde trifluoromethanesulfonate were heated, then eluted through a reverse solid-phase extraction cartridge and a column containing sodium borohydride and potassium carbonate to yield the ^{18}F-*p*-fluorobenzyl alcohol. The ^{18}F-*p*-fluorobenzyl alcohol was reacted with triphenylphosphine dibromide to produce ^{18}F-*p*-fluorobenzyl triphenyl phosphonium bromide. The yield was 6%, synthesis duration was 82 min ($n = 20$), compound purity > 99%, and specific activity was 16.7 GBq/μmol (451 mCi/μmol at end of saturated bombardment).

Cells and Loading Buffer Solution

Isolation of ventricular cardiomyocytes was performed as described (*10*). Briefly, healthy mongrel dogs of either sex were anesthetized and hearts were harvested surgically by left lateral thoracotomy, immersed in ice-cold saline, and quickly excised. The region of the ventricle was excised and perfused at 15 mL/min with Ca^{2+}-free modified Tyrode's solution at 37°C and oxygenated with 100% O_2 for 30 min; next, with the same solution with added collagenase (type I, 178 U/mL; Worthington Biochemical Corp.) and protease (type XIV, 0.12 mg/mL; Sigma) for 40 min; and next, with washout solution (with 200 μmol/L $CaCl_2$) for 15 min. Chunks of well-digested ventricular tissue from the midmyocardial layer of the ventricle were dissected out, and myocardial cells were mechanically disaggregated, filtered through nylon mesh, and stored in modified Tyrode's solution containing 2 mmol/L Ca^{2+}. The procedure yielded Ca^{2+}-tolerant quiescent cells with clear striations and no visible abnormalities (e.g., granules, blebs, etc.).

Transport Studies

Myocytes were counted with a hematocytometer and resuspended at a concentration of 2×10^6 cells per milliliter in a loading buffer solution containing 145 mmol/L NaCl, 5.4 mmol/L KCl, 1.2 mmol/L $CaCl_2$, 0.8 mmol/L $MgSO_4$, 0.8 mmol/L NaH_2PO_4, 5.6 mmol/L dextrose, and 5 mmol/L *N*-(2-hydroxyethyl)piperazine-*N*′-(2-ethanesulfonic acid), pH 7.4. Cell viability was examined by trypan blue exclusion. Viability was always >90%. Cell suspension (0.5 mL) was transferred to 1.5-mL Eppendorf Microfuge tubes and placed in 37°C water bath for 60 min before use. Uptake experiments were initiated by adding an equal volume of loading solution containing 3.7 kBq (0.1 μCi) of ^{18}F-FBnTP (final concentration, 0.5−2 nmol/L). All activities were corrected for decay. The uptake was terminated at various times by transferring 300-μL aliquots to Microfuge tubes containing 300 μL fetal calf serum and centrifuged for 1 min. Aliquots (100 μL) of the supernatant were then obtained and the remaining solution was aspirated. Microfuge tubes were placed on dry ice and their tips were cutoff just above the pellet. The radioactivity of the pellet and supernatant were assayed together with standard solution (1:1,000) in a γ-counter. Activity in serum was always <2% of total blood activity. ^{18}F-FBnTP uptake was expressed as an accumulation ratio calculated by dividing the activity in the pellet by the total radioactivity (pellet + supernatant) normalized to 10^6 cells.

Retention experiments were initiated by incubating the cells (10^6/mL) for 60 min in the loading buffer solution containing 3.7 kBq (0.1 μCi) ^{18}F-FBnTP. Cells were resuspended in an isotope-free loading solution and, at indicated times, Microfuge tubes were centrifuged for 1 min, and the activity in the pellet and supernatant was assayed, as described.

PET Acquisition

For PET studies, healthy mongrel dogs ($n = 7$; 25−35 kg body weight) were anesthetized with propofol (25−30 mg intravenously with additional supplemental doses of 5 mg, as necessary) and intubated with a cuffed endotracheal tube for mechanical ventilation with room air. During the PET scan, anesthesia was maintained by propofol infusion (5 mg/kg/min). Sterile catheters were placed in 2 leg veins for the infusion of anesthesia and injection of the radiotracer and in the femoral artery for collecting blood samples. The animals were placed in a prone position, in a specially designed holder on the PET bed, and the myocardium was centered in the scanner field of view (FOV). Blood pressure, body temperature, oxygen saturation, end-tidal CO_2, and heart rate were monitored continuously.

PET data were acquired on an Advance scanner (GE Healthcare; 35 axial slices, 4.25-mm thick, 14.4-cm axial FOV). A 10-min transmission scan using a $^{68}Ge/^{68}Ga$ source was performed for subsequent attenuation correction. After bolus administration of 126−240 MBq (3.4−6.5 mCi) ^{18}F-FBnTP via the femoral vein, a series of 23 or 26 serial PET images were acquired. The frame duration increased progressively from 15 s to 10 min until 60 min ($n = 4$) or 90 min ($n = 3$) after injection. At 0, 5, 10, 20, 30, 60, and 90 min after injection, 2-mL blood samples were collected via the femoral artery line and placed in heparinized microtubes. In 4 dogs, at the completion of a 60-min dynamic scan, a whole-body ^{18}F-FBnTP PET scan was acquired. The whole-body scan involved 4 successive bed positions, a 5-min emission scan followed by a 3-min transmission scan per bed position, starting at the most posterior position of the body and ending at the chest position overlapping the myocardial dynamic scan window. All animal protocols were approved by the Institution's Animal Care and Use Committee.

High-Performance Liquid Chromatographic (HPLC) Analysis of ^{18}F-FBnTP Metabolites

For analysis of metabolites in dogs, the 2-mL arterial blood samples were centrifuged (1,000 rpm, 1 min) and 0.5-mL plasma aliquots were collected. Plasma proteins were precipitated by mixing equal volumes of plasma and acetonitrile. After sitting on ice for 5 min, the mixture was centrifuged for 1 min in a microcentrifuge. The protein-free supernatant (0.5 mL) was diluted with water to 2 mL to reduce the acetonitrile content to approximately 12% (v/v) and was loaded into a 2-mL injector loop. The sample was chromatographed on a Prodigy C18 column (10 μm, 4.6 × 250 mm) (Phenomenex) in 60% acetonitrile:40% 100 mmol/L

triethylamine acetate buffer, pH 4.1, at a flow rate of 1 mL/min. Radioactivity was measured in a flow analyzer with bismuth germanate detectors (BioScan). The fraction of radioactivity associated with the parent compound and its metabolites were determined by integration of the respective chromatographic peaks (Laura Software; BioScan).

Image and Data Analyses

The PET scans were corrected for radioactivity decay and for attenuation using the acquired transmission scan. Image reconstruction was accomplished by filtered ordered-subset expectation maximization (OSEM; 2 iterations, 18 subsets) using a 26 × 26 cm FOV and a 256 × 256-pixel matrix, 2 × 2 mm pixel size. Serial images of the dynamic scan from 5 to 60 min were summed to produce an image for placement of a 4 × 4 mm rectangular region of interest (ROI). ROIs were placed on 3 midventricular axial images, sampling the entire circumference. A single ROI (4 × 4 mm) was placed in the middle of the left ventricular chamber. In 5 of the 7 dogs, the liver was visualized in at least 4 slices. ROIs were placed on the 3 slices most adjacent to the heart, covering most of the hepatic parenchyma. ROIs were placed on 3 successive coronal slices intersecting with the lungs, covering most of the lung parenchyma. The ROI template was then transferred to the serial images of the corresponding section, and time–activity curves were generated.

To assess the uniformity of the regional distribution of ^{18}F-FBnTP throughout the left ventricular wall, reformatting oblique slices to vertical and horizontal long-axis as well as short-axis images was performed on a Xeleris Functional Imaging workstation (GE Healthcare Technologies). Short-axis slices were used to generate polar plots and 3-dimensional volume-rendered myocardium images. In addition, radial sampling of maximum values on short-axis images summed over the 5- to 15-min and 30- to 60-min time interval after injection was performed. The image dataset was resampled to a voxel dimension of 2 × 2 × 4 mm in the *x*-, *y*-, and *z*-axis, respectively. Twenty-four sectors, 15° each, initiating at the intersection of the right ventricular wall, the interventricular septum, and the left ventricular anterior wall, counterclockwise, were placed on short-axis slices from the base to apex. Twelve to 15 short-axis slices were used for the analysis, covering most of the heart from the apex to base. The maximum value in each sector was sampled. The coefficient of variation (SD/mean) was calculated along the short (septum to anterior) and longitudinal (apex to base) axes.

Whole-body biodistribution was measured by placement of rectangular ROIs on whole-body coronal images (4-mm^3 voxel) on target organs, including the heart, liver, lung, gallbladder, muscle, bone marrow, kidney, spleen, stomach wall, and testes. For each organ, the coronal section intersecting midorgan was selected. Activity was sampled over the entire organ using rectangular ROIs (4 × 4 mm). Arterial blood activity was corrected for the metabolite fraction. Data are expressed as Bq/mL/MBq injected dose. Image-processing procedures were performed using Analyze software (AnalyzeDirect; Mayo Clinic, Rochester, MN).

RESULTS

^{18}F-FBnTP Uptake and Retention Kinetics in Isolated Myocytes

The uptake kinetics of ^{18}F-FBnTP was examined in myocytes freshly isolated from the myocardium of healthy mongrel dogs. Incubation of myocytes in the loading buffer containing ^{18}F-FBnTP resulted in a rapid time-dependent accumulation of activity and prolonged retention (Fig. 1A). At 5 and 15 min after incubation, cell-associated activity was 71% and 91% of the mean plateau activity, respectively. Resuspension of cells in isotope-free incubation medium revealed little tracer washout. At 60 and 120 min, cell-bound activity comprised 88% and 85% of control activity, respectively (Fig. 1B).

HPLC Analysis of Metabolites

^{18}F-FBnTP metabolites were observed on the chromatogram as a small radioactive peak just preceding a symmetric main peak of the parent compound eluted approximately 6 min after the column switch (Fig. 2A). No early polar peak indicative of free fluorides was detected in any given sample. The fraction of metabolites was <5% of the total activity at 5 min and increased to 8.7% at 10 min (Fig. 2B). Metabolites, as a fraction of total activity, were more significant at 20 and 30 min (17.8% and 24.1%, respectively). However, measuring the activity in the left ventricular chamber on the dynamic scans showed at 20 min after administration that the total

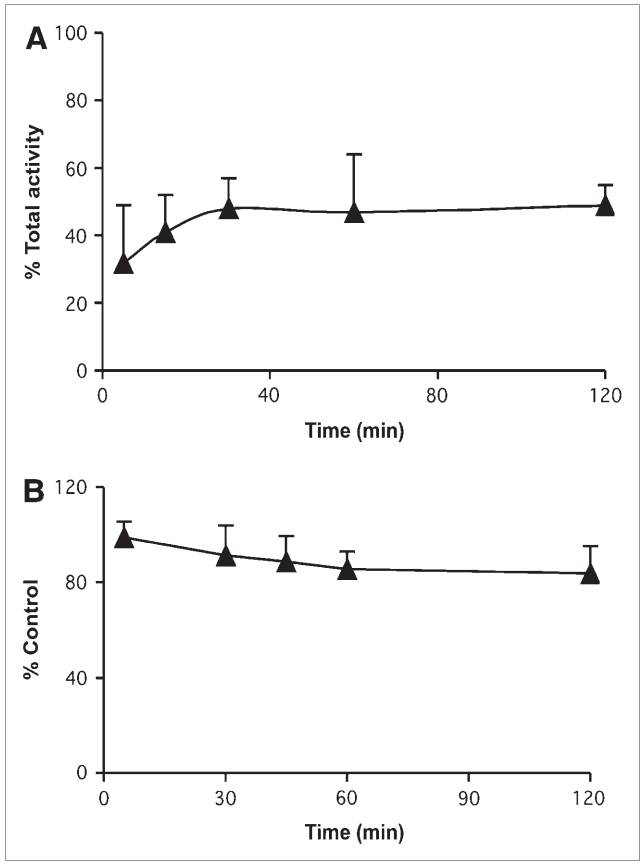

FIGURE 1. ^{18}F-FBnTP uptake (A) and retention kinetics (B) in cardiomyocytes freshly prepared from mongrel dog heart. ^{18}F-FBnTP accumulates rapidly and is retained in cells. Data represent mean ± SD of 6 determinations in 2 independent studies.

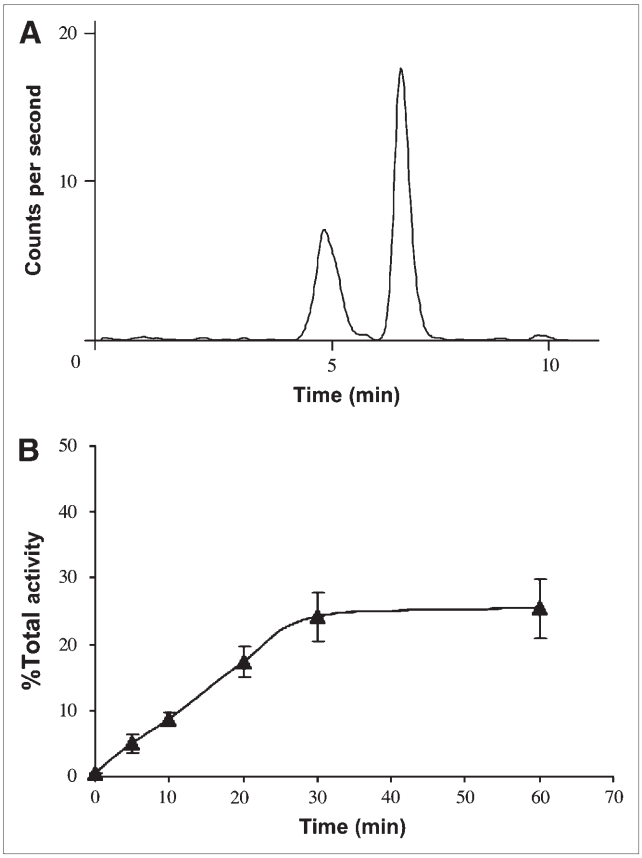

FIGURE 2. HPLC analysis of ^{18}F-FBnTP plasma metabolites. (A) Chromatogram of plasma collected 30 min after administration of ^{18}F-FBnTP. Small early peak represents metabolites; late large peak represents parent compound. (B) Metabolites in arterial blood are expressed as percentage of total plasma activity at indicated time points (mean ± SD; n = 4).

radioactivity in the blood pool was already very low, 3.2% ± 1.6% of peak activity (Fig. 3). Thus, the absolute concentration of metabolites was very low.

Extent of ^{18}F-FBnTP Defluorination

To further assess the stability of ^{18}F-FBnTP in vivo, the extent of defluorination of ^{18}F-FBnTP was examined by γ-well counting of radioactivity accumulated in the femur of CD1 mice (n = 3) at 5 and 30 min after administration. ^{18}F-FBnTP bone uptake was compared with the activity accumulated in the femur of mice (n = 3) after administration of ^{18}F-fluoride. Total bone activity was calculated under the assumption that activity in 1 femur comprises 20% of activity in total bone in mice. ^{18}F-FBnTP total bone uptake at 30 min was relatively low (1.38 percentage injected dose [%ID]) as compared with free fluoride bone uptake (15.3 %ID).

^{18}F-FBnTP Uptake and Retention Kinetics In Vivo

Similar to the fast kinetics observed in isolated cardiomyocytes in vitro, ^{18}F-FBnTP demonstrated a rapid time-dependent accumulation in the myocardium in vivo. Imaging scans of 15-s duration for the first 2 min, and 60-s scans for the following 6 min after administration, showed that ^{18}F-FBnTP activity in the left ventricular wall reached a plateau concentration within a few minutes. Figure 3 depicts the time–activity profile of ^{18}F-FBnTP in the myocardium and adjacent structures. ^{18}F-FBnTP activity in the myocardium in the scan acquired over the 15- to 30-s postadministration time interval was 68% ± 15% (mean ± SD; n = 5) of the plateau activity. The prolonged retention measured in isolated myocytes was observed in vivo as well. ^{18}F-FBnTP myocardial activity reached a plateau concentration within 5 min after administration, which was retained throughout the remaining scanning time, up to 90 min. In contrast, ^{18}F-FBnTP activity in the blood pool, as sampled in the left ventricular chamber, declined rapidly (half-life [$t_{1/2}$] = 19.5 ± 4.4 s), reaching 26.2% ± 7.8% and 13.4% ± 6.3% of activity in the left ventricular wall at 5 and 10 min, respectively.

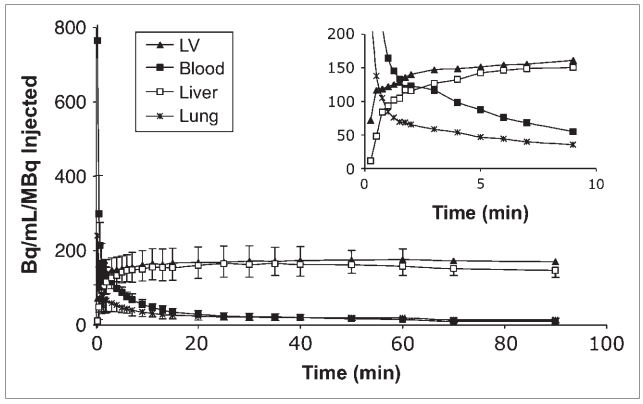

FIGURE 3. ^{18}F-FBnTP uptake kinetics in dog. Data represent mean ± SD of 7 dogs. ^{18}F-FBnTP accumulates rapidly in the left ventricular (LV) wall, reaching close to plateau value within 15–30 s (inset), but demonstrates rapid clearance of activity from blood pool and lungs. Liver kinetics resemble that of left ventricular wall.

^{18}F-FBnTP accumulation in the liver followed the time-dependent accumulation of activity observed in the myocardium (Fig. 3). Washout of liver activity was observed over the 40- to 90-min time interval. The liver mean plateau concentration over the 40- to 60-min time interval (152.6 ± 52.7 Bq/mL/MBq injected; mean ± SD, n = 5) was lower than that observed in the myocardium (173.0 ± 31.2 Bq/mL/MBq injected). The initial accumulation of ^{18}F-FBnTP in the lung parenchyma was lower than that in the myocardium. ^{18}F-FBnTP activity in the lungs rapidly declined ($t_{1/2}$ = 30.7 ± 11.6 s), reaching values observed in the blood pool within several minutes. The left ventricular wall-to-blood, wall-to-lungs, and wall-to-liver mean uptake ratios at 60 min after administration were 16.6:1, 12.2:1, and 1.2:1, respectively. The low background activity combined with the extensive uptake and prolonged retention of ^{18}F-FBnTP generated high-contrast images of the myocardium, with clear visualization of the detailed anatomy of the heart, including the papillary muscle and the left and right atria. Figure 4 depicts a representative example of ^{18}F-FBnTP PET images of a dog's myocardium summed over the 30- to 60-min interval.

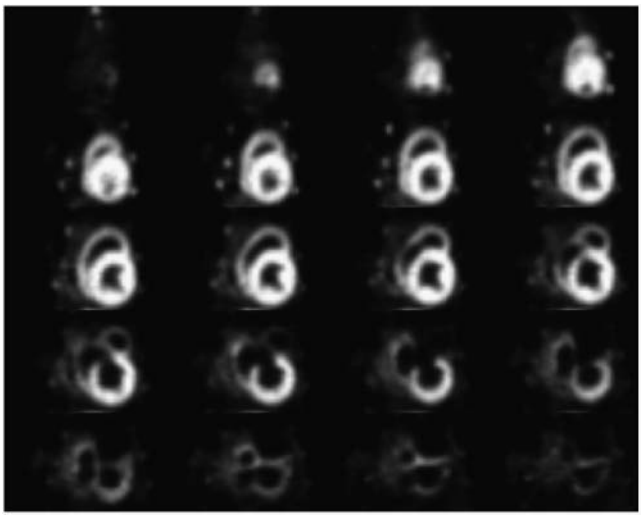

FIGURE 4. ^{18}F-FBnTP axial PET images of dog's myocardium. Images represent ^{18}F-FBnTP activity over 30–60 min after administration. Apex, upper left corner; base, lower right corner.

^{18}F-FBnTP Biodistribution in Dog Myocardium

^{18}F-FBnTP myocardial distribution was assessed qualitatively on polar maps. ^{18}F-FBnTP demonstrated uniform distribution throughout the entire myocardium. A typical example of short-axis PET images and the corresponding polar map of ^{18}F-FBnTP biodistribution in the dog's myocardium is illustrated in Figure 5. Quantitative analysis of ^{18}F-FBnTP myocardial distribution was performed by circumferential sampling of 4-mm-thick short-axis images representing the summed activity from 30 to 60 min after injection. Images selected were from the base to apex, excluding the first and last short-axis images. The coefficient of variance (SD/mean) of the circumferential profile in the short and longitudinal axes was calculated. ^{18}F-FBnTP covariance was 7.58% ± 1.01% (mean ± SD; n = 7) in the septum-to-anterior wall axis and 6.11% ± 0.89% in the apex-to-base axis. To examine the distribution of ^{18}F-FBnTP throughout the myocardial quadrants, 5 successive short-axis images intersecting the septum were selected. Figure 6A depicts the average circumferential profiles for the sampled dogs. Values were normalized to the global mean activity in each dog. Similar activity was observed in the septal (1.03 ± 0.06, mean ± SD; n = 7), inferior (1.01 ± 0.09), lateral (0.99 ± 0.06), and anterior (1.01 ± 0.05) walls (P value for septal vs. other quadrants > 0.192).

In view of the rapid accumulation and equilibration of ^{18}F-FBnTP activity in the myocardium, the pattern of distribution was examined on images representing the activity summed over 5−15 min after injection. ^{18}F-FBnTP activity on the early, short images demonstrated a uniform distribution profile throughout the entire myocardium, similar to that observed on the delayed, prolonged (30−60 min) images. The mean distribution covariance was 7.25% ± 1.43% in the short axis and 6.12% ± 1.88% in the longitudinal axis. Figure 6B depicts the circumferential profile in 5 short-axis slices intersecting the septum. A uniform distribution was observed throughout the septal (1.02 ± 0.05, mean ± SD; n = 7), inferior (1.05 ± 0.08), lateral (0.98 ± 0.04), and anterior (0.98 ± 0.03) walls (P value for inferior vs. other quadrants > 0.116). The corresponding short-axis images are shown on the right side of Figures 6A and 6B. As can be seen, summation of ^{18}F-FBnTP activity over the 5- to 15-min postinjection interval generated high-contrast cardiac images. The quality of the 5- to 15-min images is similar to that of the 30- to 60-min images.

Whole-Body Biodistribution

^{18}F-FBnTP whole-body distribution was examined in 4 dogs. ^{18}F-FBnTP demonstrated a highly organ-specific uptake. Figure 7 shows a representative example of whole-body ^{18}F-FBnTP PET coronal images acquired in a mongrel dog. The following structures can be seen: left and right ventricles, left atrium, liver and gallbladder, stomach wall, small intestine, spleen, kidney, colorectal wall, and testes. The kidney was the major target organ of ^{18}F-FBnTP. A sharp distinction between the kidney cortex and medulla aspects was observed, with the cortex-to-medulla uptake ratio of 8.73 ± 1.78 (mean ± SD; n = 4). Intense activity was observed in the gallbladder. Similar activity was observed in the heart and liver. Low organ-specific activity was measured in the bone, spleen, and lung. The ^{18}F-FBnTP organ uptake and left ventricular wall-to-organ uptake ratio are summarized in Table 1.

DISCUSSION

This study was aimed at characterizing the uptake kinetics and biodistribution of the novel PET agent ^{18}F-FBnTP and to

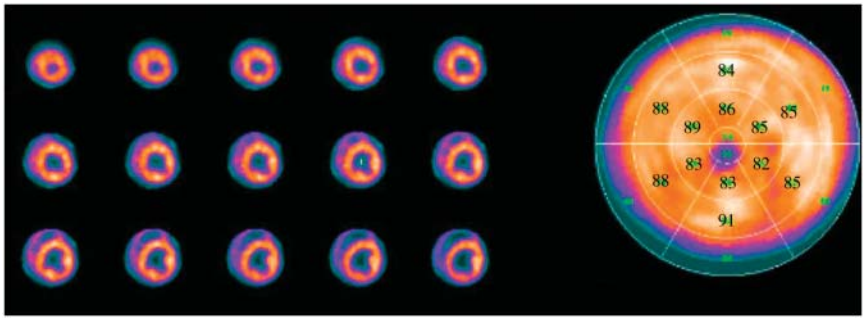

FIGURE 5. Representative example of short-axis PET images and polar map of ^{18}F-FBnTP biodistribution in myocardium of healthy mongrel dog.

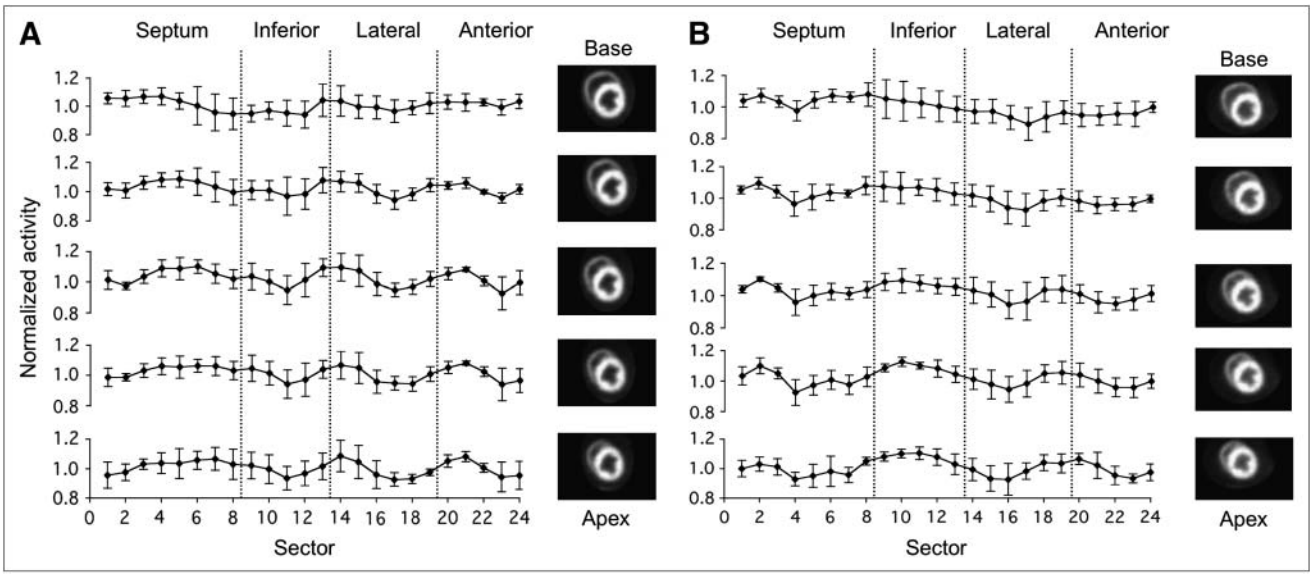

FIGURE 6. Circumferential profiles of ^{18}F-FBnTP activity in 5 successive short-axis images intersecting the septum (4-mm slice thickness). Activity profiles are mean ± SD of 7 dogs. Values represent activity normalized to a global mean per dog. (A) Profiles of summed activity over 30–60 min after injection. (B) Profiles of summed activity over 5–15 min after injection. Corresponding short-axis slices, taken from 1 dog, are depicted to right of activity profiles. A uniform activity profile is observed in all left ventricular wall quadrants. Similar distribution profile and image quality are observed in short, early scans and prolonged, delayed scans.

assess its suitability as an imaging agent of the myocardium. The findings obtained in this study indicate that ^{18}F-FBnTP has several characteristics that are essential for a good cardiac imaging PET radioligand. These include (a) metabolic stability and minimal defluorination; (b) rapid and intense accumulation and prolonged retention in myocytes, both in vitro and in vivo; (c) ability to yield high-quality images by a short (10 min) scan acquired early after injection (5 min); (d) uniform distribution throughout the entire myocardium; (e) fast clearance of background activity (from the blood pool and lungs); and (f) liver uptake not exceeding that in the heart.

^{18}F-FBnTP is a member of the class of potentiometric lipophilic phosphonium cations, originally developed for measurement of the mitochondrial membrane potential (*11*). The lipophilic nature and delocalized positive charge enable the cation to cross the lipid bilayer by passive diffusion and accumulate in cells in a membrane potential−dependent manner. Because of the greater membrane potential, the cation accumulates mainly in the mitochondrion (*12*). In vitro pharmacologic analysis showed that ^{18}F-FBnTP accumulation in cells is dependent primarily on the mitochondria membrane potential. Selective abolishment of the

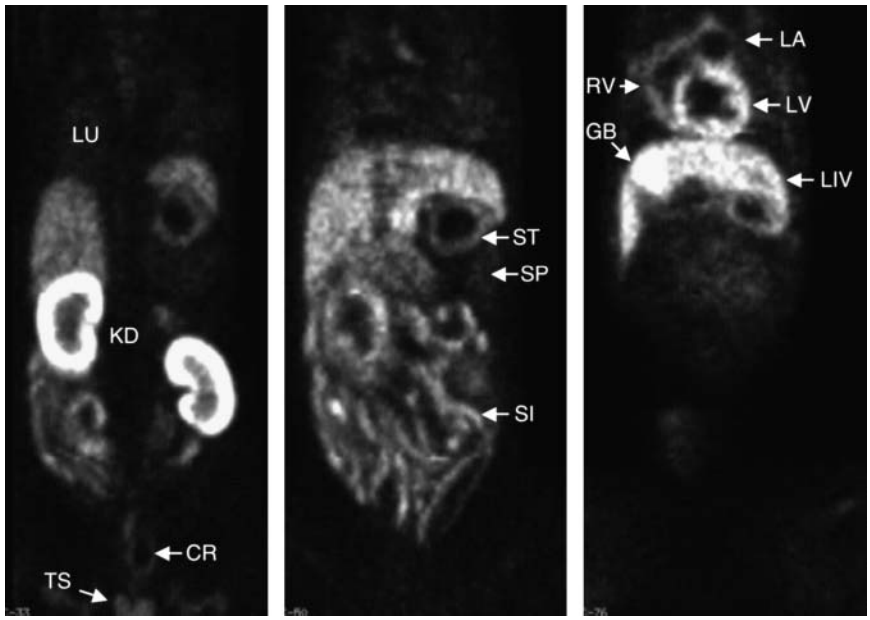

FIGURE 7. Whole-body distribution of ^{18}F-FBnTP in healthy mongrel dog. PET images were acquired in 4 consecutive bed positions (5-min emission, 3-min transmission scan per bed position). Despite the short scan duration, high organ-specific accumulation of ^{18}F-FBnTP enables a clear visualization of left ventricular (LV), right ventricular (RV), and left atrium (LA) walls, cortical and medulla aspects of kidney (KD), liver (LIV), and gallbladder (GB), stomach wall (ST), small intestine (SI), colorectal segment (CR), and testes (TS). Low uptake is observed in spleen (SP) and lungs (LU). Heart and liver demonstrate similar uptake at 90 min after administration.

TABLE 1
Whole-Body Distribution of ^{18}F-FBnTP in Dogs

Organ	Bq/mL/MBq injected	LV-to-organ ratio
LV wall	171.60 ± 21.6	
RV wall	86.63 ± 25.8	1.93 ± 0.60
LV chamber	9.86 ± 4.0	18.49 ± 8.80
RV chamber	11.34 ± 4.4	15.46 ± 5.77
Aorta	10.25 ± 4.2	17.50 ± 7.89
Lung	12.02 ± 2.2	13.45 ± 3.62
Liver	147.70 ± 25.4	1.16 ± 0.08
Gallbladder	259.25 ± 44.7	0.61 ± 0.10
Spleen	19.15 ± 8.8	9.52 ± 4.37
Stomach wall	73.91 ± 26.4	2.36 ± 0.93
Kidney cortex	594.12 ± 136.4	0.27 ± 0.05
Kidney medulla	68.03 ± 3.3	2.30 ± 0.34
Bone	42.07 ± 19.5	4.50 ± 2.63
Colorectal wall	23.30 ± 18.9	6.24 ± 3.64
Testes	94.26 ± 8.2	1.66 ± 0.21

LV = left ventricular; RV = right ventricular.
Data are mean ± SD (n = 4).

mitochondria membrane potential resulted in a decrease of cell-bound activity of >80% (*13*).

SPECT studies have shown that targeting the mitochondria using potentiometric probes constitutes a successful approach for cardiovascular imaging. Accordingly, the mitochondria-targeting cationic technetium complexes ^{99m}Tc-sestamibi and ^{99m}Tc-tetrofosmin are the mainstay of MPI in clinical diagnostic studies of CAD. Conventional SPECT is highly sensitive for the detection of multivessel coronary disease (90%−94%) but of limited sensitivity (60%−70%) in single-vessel disease (*14,15*). An important reason for the reduced sensitivity is artifacts introduced because of suboptimal tracer distribution in organs adjacent to the myocardium. Intense liver uptake, caused by prominent hepatobiliary excretion, is frequently observed on ^{99m}Tc-sestamibi and ^{99m}Tc-tetrofosmin images (*16,17*). Dynamic SPECT studies of ^{99m}Tc-tetrofosmin in mongrel dogs have shown that the liver uptake is 2.5 and 1.7 times greater than the heart activity at 5 and 30 min, respectively (*18*). More intense liver uptake of ^{99m}Tc-tetrofosmin has been measured at rest in humans (*19*). ^{99m}Tc-Sestamibi liver uptake is greater and activity washout is slower than that of ^{99m}Tc-tetrofosmin (*17,19*). High liver uptake would result in photon scatter that may mask the detection of flow abnormalities, particularly in the inferior and inferoapical left ventricular wall (*20,21*).

In our experimental study, the ^{18}F-FBnTP accumulation in the liver did not exceed the activity measured in the left ventricular wall. The better heart-to-liver uptake ratio of ^{18}F-FBnTP, compared with technetium complexes, suggests less photon scatter from the liver. The lack of an effect of liver radioactivity on the left ventricular wall was demonstrated by the uniform distribution of ^{18}F-FBnTP throughout the entire myocardium, including the inferior aspect adjacent to the liver.

To avoid photon scatter from the liver on SPECT, a delayed scan to allow clearance of activity from the liver and gallbladder to the gastrointestinal area is recommended (*22,23*). Other means (e.g., high-lipid foods) for reducing liver and gallbladder uptake of technetium complexes were tested with partial success (*24*). In the present study, the gallbladder of a few dogs (n = 3) was in the imaging window of the dynamic scan. The kinetics data showed that the ^{18}F-FBnTP gallbladder uptake is relatively low for the first 50 min after injection (heart/gallbladder > 1.47) and surpasses the heart activity at 60 min (heart/gallbladder = 0.69). Whole-body imaging showed that the kidney is the major target organ of ^{18}F-FBnTP. The kidney uptake was 4 times greater than the activity measured in the liver. These data suggest that ^{18}F-FBnTP is washed out more from the body via the renal tract than from the hepatobiliary tract. Renal clearance is a more favorable tract for cardiac imaging studies.

An additional factor that may affect image quality and the sensitivity of the diagnostic test to detect coronary flow defects in the left ventricular wall is the background activity generated primarily by the tracer residing in the blood pool and the lungs. ^{18}F-FBnTP activity cleared very rapidly from the lungs, at a rate similar to that observed in the left ventricular cavity. A heart-to-lung uptake ratio of 12:1 was obtained within 5 min. This ratio is much greater than that reported for ^{99m}Tc-tetrofosmin in mongrel dogs (2:1) (*18*). The better heart-to-lung ratio suggests lower background activity and, consequently, better image contrast for ^{18}F-FBnTP than the technetium complex.

The rapid accumulation, distribution, and equilibration of ^{18}F-FBnTP activity in the myocardium, combined with the rapid clearance of background activity from the blood pool and lungs, allow acquisition of high-contrast images using a relatively short scan (10 min in duration) early after the intravenous administration of the radioisotope. This may allow better patient management compared with protocols of MPI studies using SPECT in the clinical setting.

Image uniformity is a crucial factor in identifying functional defects in the myocardium. Despite current major efforts to develop algorithms for attenuation correction for SPECT, a standardized method for conventional clinical studies has not yet been developed. Lack of attenuation correction was shown to be the culprit of false-positive results during SPECT perfusion studies, resulting in a specificity as low as 40% in obese subjects (*2*). A multicenter trial using ^{201}Tl and ^{99m}Tc-tetrofosmin reported low sensitivity (35%−40%) and specificity (48%−50%) in detecting a flow defect in the lateral and inferoapical walls, respectively (*25*). Coronary angiography served as a gold standard. The lateral and inferoapical walls are particularity susceptible to artifacts caused by photon attenuation and scatter.

In contrast, ^{18}F-FBnTP demonstrated uniform distribution throughout the entire myocardium, including the inferior aspect. The high uniformity of ^{18}F-FBnTP distribution in the

left ventricular wall may be attributed to the relatively low extracardiac uptake and the ability to perform nonuniform attenuation correction on PET images. ^{18}F-FBnTP distribution covariance (SD/mean) was in the range of 6%−8% in the short and longitudinal axes. This suggests the potential of detecting regional decreases of ^{18}F-FBnTP myocardial activity as small as 10% with confidence greater than 68%, using PET. Furthermore, ^{18}F-FBnTP may provide a sensitive means for detecting small flow defects with similar accuracy throughout the myocardium, including the inferior aspect.

CONCLUSION

^{18}F-FBnTP is a new radiopharmaceutical demonstrating features that are well suited for cardiac imaging, including rapid kinetics, uniform distribution in the left ventricular wall, and favorable organ distribution. These characteristics suggest that ^{18}F-FBnTP PET may afford an accurate noninvasive means for diagnosing small flow defects undetected by current diagnostic tests and improving MPI protocols in the clinical setting.

ACKNOWLEDGMENTS

The authors thank David Clough for acquisition of the PET scans and Jeff Brawn for preparation of the dogs. This work was supported in part by a grant from The Johns Hopkins University School of Medicine Institute for Cell Engineering, National Institute of Health grants U54 HL081028 (Specialized Center for Cell-Based Therapy), R21 HL-72185, RO1 HL-65455, and RO1 AG-025017, and The Donald W. Reynolds Foundation.

REFERENCES

1. Beller GA, Bergmann SR. Myocardial perfusion imaging agents: SPECT and PET. *J Nucl Cardiol.* 2004;11:71–86.
2. Dondi M, Fagioli G, Salgarello M, et al. Myocardial SPECT: what do we gain from attenuation correction (and when)? *Q J Nucl Med Mol Imaging.* 2004; 48:181–187.
3. Dayanikli F, Grambow D, Muzik O, et al. Early detection of abnormal coronary flow reserve in asymptomatic men at high risk for coronary artery disease using positron emission tomography. *Circulation.* 1994;90:808–817.
4. Di Carli MF, Janisse J, Grunberger G, Ager J. Role of chronic hyperglycemia in the pathogenesis of coronary microvascular dysfunction in diabetes. *J Am Coll Cardiol.* 2003;41:1387–1393.
5. Machac J. Cardiac positron emission tomography imaging. *Semin Nucl Med.* 2005;35:17–36.
6. Krivokapich J, Smith GT, Huang SC, et al. N-13 ammonia myocardial imaging at rest and with exercise in normal volunteers: quantification of absolute myocardial perfusion with dynamic positron emission tomography. *Circulation.* 1989; 80:1328–1337.
7. Schelbert HR, Phelps ME, Huang SC, et al. N-13 ammonia as an indicator of myocardial blood flow. *Circulation.* 1981;63:1259–1272.
8. Krause BJ, Szabo Z, Becker LC, et al. Myocardial perfusion with [^{11}C]methyl triphenyl phosphonium: measurements of the extraction fraction and myocardial uptake. *J Nucl Biol Med.* 1994;38:521–526.
9. Ravert HT, Madar I, Dannals RF. Radiosynthesis of 3-[^{18}F]-fluoropropyl and 4-[^{18}F]-fluorobenzyl triarylphosphonium ions. *J Labelled Compds Radiopharm.* 2004;47:469–475.
10. O'Rourke B, Kass DA, Tomaselli GF, et al. Mechanisms of altered excitation-contraction coupling in canine tachycardia-induced heart failure. I. experimental studies. *Circ Res.* 1999;84:562–570.
11. Grinius LL, Jasaitis AA, Kadziauskas YP, et al. Conversion of biomembrane-produced energy into electric form. I. submitochondrial particles. *Biochim Biophys Acta.* 1970;216:1–12.
12. Murphy MP. Selective targeting of bioactive compounds to mitochondria. *Trends Biotechnol.* 1997;15:326–330.
13. Madar I, Ravert HT, Nelkin B, et al. Physiochemical characteristics and uptake kinetics of the voltage indicator [F-18]phosphonium cations [abstract]. *J Nucl Med.* 2003;44(suppl):14P.
14. Kong BA, Shaw L, Miller DD, Chaitman BR. Comparison of accuracy for detecting coronary artery disease and side-effect profile of dipyridamole thallium-201 myocardial perfusion imaging in women versus men. *Am J Cardiol.* 1992;70:168–173.
15. Nishimura S, Mahmarian JJ, Boyce TM, Verani MS. Quantitative thallium-201 single-photon emission computed tomography during maximal pharmacologic coronary vasodilation with adenosine for assessing coronary artery disease. *J Am Coll Cardiol.* 1991;18:736–745.
16. Nakajima K, Taki J, Shuke N, Bunko H, Takata S, Hisada K. Myocardial perfusion imaging and dynamic analysis with technetium-99m tetrofosmin. *J Nucl Med.* 1993;34:1478–1484.
17. Okada RD, Glover D, Gaffney T, Williams S. Myocardial kinetics of technetium-99m-hexakis-2-methoxy-2-methylpropyl-isonitrile. *Circulation.* 1988;77:491–498.
18. Sinusas AJ, Shi Q, Saltzberg MT, et al. Technetium-99m-tetrofosmin to assess myocardial blood flow: experimental validation in an intact canine model of ischemia. *J Nucl Med.* 1994;35:664–671.
19. Higley B, Smith FW, Smith T, et al. Technetium-99m-1,2-bis[bis(2-ethoxyethyl) phosphino]ethane: human biodistribution, dosimetry and safety of a new myocardial perfusion imaging agent. *J Nucl Med.* 1993;34:30–38.
20. Nuyts J, Dupont P, Van den Maegdenbergh V, Vleugels S, Suetens P, Mortelmans L. A study of the liver-heart artifact in emission tomography. *J Nucl Med.* 1995; 36:133–139.
21. Kailasnath P, Sinusas AJ. Comparison of Tl-201 with Tc-99m-labeled myocardial perfusion agents: technical, physiologic, and clinical issues. *J Nucl Cardiol.* 2001;8:482–498.
22. Matsunari I, Fujino S, Taki J, et al. Impaired fatty acid uptake in ischemic but viable myocardium identified by thallium-201 reinjection. *Am Heart J.* 1996; 131:458–465.
23. Boz A, Gungor F, Karayalcin B, Yildiz A. The effects of solid food in prevention of intestinal activity in Tc-99m tetrofosmin myocardial perfusion scintigraphy. *J Nucl Cardiol.* 2003;10:161–167.
24. Hurwitz GA, Clark EM, Slomka PJ, Siddiq SK. Investigation of measures to reduce interfering abdominal activity on rest myocardial images with Tc-99m sestamibi. *Clin Nucl Med.* 1993;18:735–741.
25. Zaret BL, Rigo P, Wackers FJ, et al. Myocardial perfusion imaging with ^{99m}Tc-tetrofosmin: comparison to ^{201}Tl imaging and coronary angiography in a phase III multicenter trial—^{99m}Tc-Tetrofosmin International Trial Study Group. *Circulation.* 1995;91:313–319.

JNM The Journal of NUCLEAR MEDICINE

Characterization of Uptake of the New PET Imaging Compound ^{18}F-Fluorobenzyl Triphenyl Phosphonium in Dog Myocardium

Igal Madar, Hayden T. Ravert, Yong Du, John Hilton, Lana Volokh, Robert F. Dannals, James J. Frost and Joshua M. Hare

J Nucl Med. 2006;47:1359-1366.

The Journal of Nuclear Medicine is published monthly.
SNMMI | Society of Nuclear Medicine and Molecular Imaging
1850 Samuel Morse Drive, Reston, VA 20190.
(Print ISSN: 0161-5505, Online ISSN: 2159-662X)

SNMMI SOCIETY OF NUCLEAR MEDICINE AND MOLECULAR IMAGING